Petroleum Science 21 (2024) 1539–1551

Contents lists available at ScienceDirect

Petroleum Science

journal homepage: www.keaipublishing.com/en/journals/petroleum-science

Original Paper

Impact of volcanism on the formation and hydrocarbon generation of organic-rich shale in the Jiyang Depression, Bohai Bay Basin, China

Jia-Hong Gao [a, 1], Xin-Ping Liang [a, 1, *], Zhi-Jun Jin [a, b, **], Quan-You Liu [a], Chang-Rong Li [a], Xiao-Wei Huang [a, c], Ju-Ye Shi [c], Peng Li [b]

[a] State Key Laboratory of Shale Oil and Gas Enrichment Mechanisms and Efficient Development, Institute of Energy, Peking University, Beijing, 100871, China
[b] Petroleum Exploration and Production Research Institute, SINOPEC, Beijing, 100083, China
[c] School of Energy Resources, China University of Geosciences, Beijing, 100083, China

ARTICLE INFO

Article history:
Received 11 January 2023
Received in revised form
17 September 2023
Accepted 18 January 2024
Available online 21 January 2024

Edited by Jie Hao and Meng-Jiao Zhou

Keywords:
Volcanic ash
Hydrocarbon generation
Organic-rich shale
Shahejie Formation
Jiyang Depression

ABSTRACT

Globally, most organic-rich shales are deposited with volcanic ash layers. Volcanic ash, a source for many sedimentary basins, can affect the sedimentary water environment, alter the primary productivity, and preserve the organic matter (OM) through physical, chemical, and biological reactions. With an increasing number of breakthroughs in shale oil exploration in the Bohai Bay Basin in recent years, less attention has been paid to the crucial role of volcanic impact especially its influence on the OM enrichment and hydrocarbon formation. Here, we studied the petrology, mineralogy, and geochemical characteristics of the organic-rich shale in the upper submember of the fourth member (Es_4^1) and the lower submember of the third member (Es_3^3) of the Shahejie Formation, aiming to better understand the volcanic impact on organic-rich shale formation. Our results show that total organic carbon is higher in the upper shale intervals rich in volcanic ash with enriched light rare earth elements and moderate Eu anomalies. This indicates that volcanism promoted OM formation before or after the eruption. The positive correlation between Eu/Eu* and Post-Archean Australian Shale indicates hydrothermal activity before the volcanic eruption. The plane graph of the hydrocarbon-generating intensity (S_1+S_2) suggests that the heat released by volcanism promoted hydrocarbon generation. Meanwhile, the nutrients carried by volcanic ash promoted biological blooms during Es_4^1 and Es_3^3 deposition, yielding a high primary productivity. Biological blooms consume large amounts of oxygen and form anoxic environments conducive to the burial and preservation of OM. Therefore, this study helps to further understand the organic-inorganic interactions caused by typical geological events and provides a guide for the next step of shale oil exploration and development in other lacustrine basins in China.

1. Introduction

Shale oil refers to the oil present in organic shale formations, which includes oil in the pores and fractures of shale, as well as oil in tight carbonate and clastic interlayers (Jin et al., 2019, 2021). The development of shale oil depends on the horizontal well staged fracturing technology (Jin et al., 2019). Recent studies have shown that most organic-rich shale intervals are deposited with volcanic ash layers, such as the Bazhenov Formation in the West Siberia Basin in Russia (Liang et al., 2021), upper Devonian in the Williston Basin and Carboniferous Bakken Formation in the US (Dennison and Textoris, 1970), Jurassic Vaca Muerta Formation in the Neuquen Basin of Argentina (Diego et al., 2014; Kietzmann and Palma, 2014), Chang 7 Formation in the Ordos Basin (Liu et al., 2021), Wufeng–Longmaxi Formation in the Sichuan Basin (Zhao et al., 2015), and Lucaogou Formation in the Junggar Basin (Wu et al., 2012).

Volcanic ash is a source for many sedimentary basins (Batchelor, 2003; Li et al., 2014; Wu et al., 2018). During the subsidence of volcanic ash, mantle hydrothermal fluids with high temperature and pressure change the physical field of the formation of organic-rich shale (Kuypers et al., 2002; Leckie et al., 2002; Liao et al., 2016).

* Corresponding author.
** Corresponding author.
E-mail addresses: xinping.liang@pku.edu.cn (X.-P. Liang), jinzj1957@pku.edu.cn (Z.-J. Jin).
[1] These authors contributed equally to this work.

https://doi.org/10.1016/j.petsci.2024.01.017

The entry of carbon sources, nutrients, and trace metals into the water column changes the chemical field and causes the bloom of algae and bacteria as well, thus changing the biological field (Little et al., 1997; Verati et al., 1999; Duggen et al., 2007; Dick et al., 2013; Du et al., 2022). Furthermore, the nutrients and trace metals carried by the volcanic ash provide a material basis for improving the primary productivity of the water column (Demaison and Moore, 1980; Haydon et al., 2006; Zhang et al., 2018; Edmonds et al., 2022). Simultaneously, the oxygen content in the water column decreases, transitioning the water column environment from weakly oxidizing to strongly reducing after a volcanic eruption (Gao et al., 2018; Lee et al., 2018; Zou et al., 2019). Organic matter (OM) oxidation and degradation are inhibited in strongly reducing environments, thereby promoting the efficiency of OM conservation (Liu et al., 2018; Liu et al., 2022b; Hong et al., 2019a,b).

The Jiyang Depression is a typical Mesozoic–Cenozoic continental rift basin in eastern China and the earliest oil and gas discovery area in the Bohai Bay Basin. In 1961, well Hua 8 obtained industrial oil flow. After nearly 60 years of exploration and development, the proven rate of oil resources has reached 52.1% and the average exploratory well density has exceeded 0.23 wells/km^2 (Guo, 2011). Shale oil resources are essential for increasing reserves and stabilising production (Song and Li, 2020). Previous research on the Jiyang Depression was based on the characteristics of the source rocks and geochemical evaluation (Pan et al., 2016; Liu, 2022). The main reason for the rich OM content of the upper submember of the fourth member (Es_4^1) and the lower submember of the third member (Es_3^3) of the Shahejie Formation in the Jiyang Depression was determined to be a continental rift basin in a saline lake sedimentary environment. Core observations show layered volcanic ash in the organic-rich shale intervals. Significant volcanism has been reported from the Late Jurassic to the Eocene in the Jiyang Depression (Wang et al., 1994; Liu et al., 2022a, 2022c). The fine-grained pyrite and increased Sr/Ba values above the tuff layer indicate that volcanism may have caused the intermittent reduction environment and salinisation of the water volume in the Shahejie Formation (Tian et al., 2020; Zhou et al., 2020; Liu et al., 2022a, 2022c). However, less attention has been paid to volcanic impacts on hydrocarbon generation and the formation of organic-rich shales in the Jiyang Depression.

Therefore, in this study, we focused on the typical organic-rich shales of Es_4^1 and Es_3^3 in the Jiyang Depression and analysed the impact of volcanic activity on the formation, preservation, and hydrocarbon generation of tuffaceous organic-rich shales by studying their petrological and geochemical characteristics. This study may provide a guide for the next step of shale oil exploration and development not only in the Bohai Bay Basin but also in other lacustrine basins of China.

2. Geological setting

The Jiyang Depression is located in the southeast Bohai Bay Basin and is bordered by the Chengning and Luxi uplifts (Wang et al., 2019). The Jiyang Depression consists of a few half-graben sags (Hou et al., 1998) and four sags: Dongying, Huimin, Zhanhua, and Chezhen from south to north (Wang et al., 2004) (Fig. 1(a) and (b)).

The strata in the Jiyang Depression developed during the Palaeozoic, Mesozoic, and Cenozoic. The Palaeozoic strata mainly compose the basement of the basin, which is primarily Cambrian–Ordovician marine carbonate rock and Carboniferous–Permian period sea–land interaction sand mudstone. The Mesozoic basement is composed of terrigenous clastic rocks. Cenozoic deposits constitute the caprock of the basin and include Paleogene, Neogene, and Quaternary deposits. The Paleogene includes the Kongdian (Ek), Shahejie (Es), and Dongying (Ed) Formations. The Neogene includes the Guantao (Ng) and Minghuazhen (Nm) Formations. The Quaternary includes the Pingyuan Formation (Q). The main research objects of this study were the upper fourth submember (Es_4^1) and the lower third submember (Es_3^3) of the Shahejie Formation in the Middle Eocene (Fig. 1(c)). Es_4^1 developed to a thickness of 100–350 m. The sedimentary facies are mainly deltas and beach bars on the edge of the gentle slope zone in the south, and deltas and nearshore underwater fans on the edge of the steep slope zone in the north. The lithology of the lower Es_4^1 interval is dominated by interbedded grey, blue-grey, grey-green mudstone; light-grey dolomitic gravel-bearing sandstone; and calcareous mudstone. The lithology of the upper Es_4^1 interval is grey-brown and dark-grey mudstone, limestone, and argillaceous limestone with biological limestone, dolomite, and gypsum interlayers. During the depositional period of Es_3^3, the climate changed from dry and hot to warm and humid, with abundant rainfall, expanded lake area, maximum water depth, and the most developed semi-deep lake–deep lake sediments (Wang et al., 2015; Liang et al., 2017). The lithology of this section is dominated by dark-grey and oil-rich mudstones with small amounts of limestone, dolomite, and unequal-grained conglomerate sandstone caused by slump gravity flow. The organic-rich shales in this section are well-developed, widely distributed, and are 100–400 m thick, making them the most favourable high-quality oil source rocks in the depression.

The Dongying Sag was formed during the Mesozoic and Cenozoic. On the west, it is bounded by the Qingcheng Uplift and Linjiafan structures and is connected to the Huimin Depression. The northern side is bounded by the Zhanhua Depression. Laizhou Bay, connected to the Qingdong Sag, is situated on its eastern side. The Dongying Sag is approximately 150 km long from east to west, 74 km wide from north to south, and covers an approximate area of 5700 km^2 (Fan, 2016). The Qingdong Sag is a Cenozoic strike-slip pull-apart basin controlled by a regional tensile stress field and the Tan-Lu Fault (Yang, 2011). Generally, the maturity of the source rocks in the sag is relatively low, and the deep sag zone exhibits the highest degree of evolution. The maturity of the source rocks in Es_4^1 is higher than that in Es_3^3 (Liu, 2016). The Fulin Sag is a small sedimentary sag in the southeastern corner of the Zhanhua Sag in the Jiyang Depression. Its northern edge is the Kenli Fault Zone, separated from the Gunan Sag. The Kendong Fault Zone, adjacent to the Kendong and Qingtuozi uplifts, covers the eastern side. The Chenjiazhuang Uplift is present on the southwest with the north and northeast faults. A tertiary fault depression with an area of approximately 360 km^2 is located southwest of the Fulin Sag (Hou, 2008).

3. Samples and methods

Forty organic-rich shale samples were collected from Es_4^1 and Es_3^3 of six wells in the Jiyang Depression: QD25 in the Qingdong Sag, Fu117 and Fu29 in the Fulin Sag, and F120, and W111 in the Dongying Sag. Moreover, 191 consecutive samples were taken between 3052.9 m and 3430.5 m (with an interval of 2 m) in the FY1 well of the Dongying Sag (Fig. 1(b)). For all samples, petrological and geochemical characteristics were analysed, including thin-section observations, total organic carbon (TOC), pyrolysis, and major- and trace-element analyses.

Samples were trimmed to remove visible veins and weathered surfaces and pulverized to a size of ~200-mesh in an agate mortar for geochemical analysis. A magnetic susceptibility instrument, KT-10, was used to precisely test the magnetic susceptibility of wells QD25 and Fu117. The thin-section analysis applied a combination of ordinary optical electron microscopy (Leica Model DM4 P) and

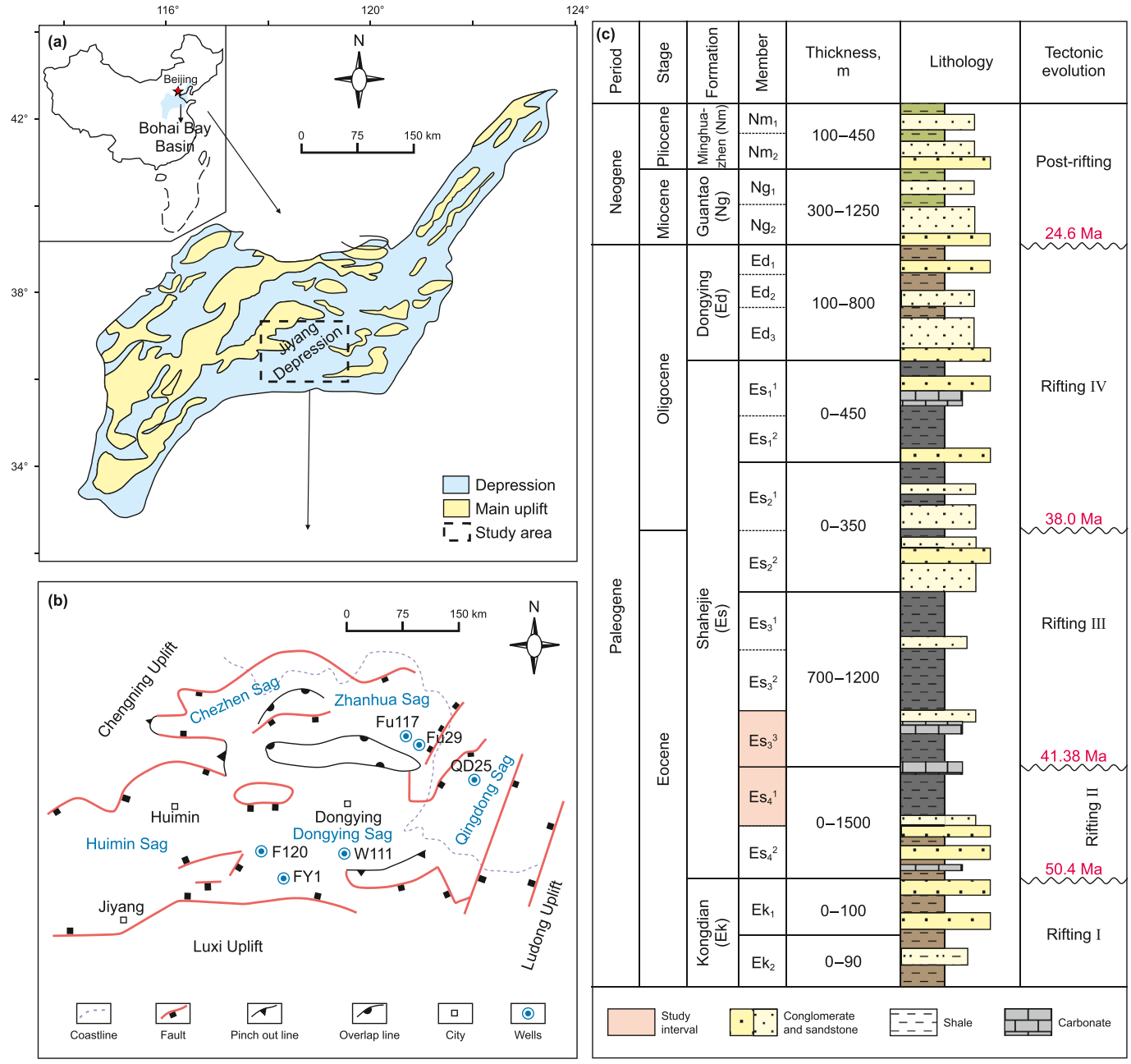

Fig. 1. Location and sedimentary background of the study area. **(a)** Geological background map of the Jiyang Depression in the Bohai Bay Basin. **(b)** The structure of Jiyang Depression. The F120, FY1, and W111 in Dongying Sag; the QD25 in Qingdong Sag; and the Fu117 and Fu29 in Zhanhua Sag. **(c)** Comprehensive stratigraphic column of this area (modified from Shi et al., 2020).

electron probe point-line-surface methods to identify the elements in the tuffaceous shale. Parts of the samples selected for TOC analysis were treated with 4.5% hydrochloric acid to eliminate inorganic carbon, and other parts of the samples were not subjected to acid treatment. The samples were then combusted at a high temperature (1250 °C) in an oxygen-enriched atmosphere to measure TOC, which was carried out in a Skyray CS-188 carbon-sulphur analyser. X-ray diffraction (XRD) was conducted using a D2-Advance instrument. Samples were ground to a size of 200-mesh with an agate mortar and then tested for full rock mineral contents. Residual (S_1) and pyrolysis hydrocarbons (S_2) were obtained via rock pyrolysis. Rock-Eval pyrolysis was conducted on the powdered samples using a Rock-Eval VI instrument. The content of the free hydrocarbon S_1 was measured at 300 °C, and the generated hydrocarbon S_2 was identified at a temperature of 600 °C. Major- and trace-element analyses were conducted at the China University of Geosciences (Wuhan, China). A Philips PW 2404 X-ray fluorescence (XRF) spectrometer was used to analyse the major elemental contents. The sample was first heated in a muffle furnace at 105 °C for 4 h. Then, anhydrous lithium tetraborate (~5.2 g), lithium fluoride (~0.4 g), and ammonium nitrate (~0.3 g) were added and dissolved at 1150 °C for another 15 min to measure the content of major oxides and loss on ignition. To determine the trace-element content, the homogenised powder-digested samples were analysed using spectroscopic methods (inductively coupled plasma mass spectrometry [ICP-MS]; Element XR). To determine trace elements,

powered samples (~25 mg) were dissolved in a mixture of hydrofluoric acid (1 mL) and nitric acid (0.5 mL) in a tightly sealed Teflon bomb at 185 °C for 24 h. The dissolved samples were diluted to 25 mL in a clean bottle for trace element analyses using a Finnigan MAT high-resolution inductively coupled plasma mass spectrometer. Additionally, the accuracy of the measurements was ensured by using standard materials and repeated analyses.

4. Results

4.1. Petrological features

A positive grain order is observed in Well QD25, which transition from tuffaceous conglomerate to tuffaceous mudstone from the bottom-up (Fig. 2(a)–(g)). The organic-rich shale intervals include mudstones, shale, calcareous mudstone, argillaceous limestone, argillaceous siltstone, silty mudstone, siltstone, limestone, and dolomite. The carbonate mineral content, primarily calcite, is relatively high. Quartz, feldspar, and clay minerals, as well as traces of pyrite, were also noted (Fig. 3(a)–(i)). The clay minerals are mainly illite/smectite (I/S). Multiple sets of tuff interlayers, such as assemblages of tuffaceous sandstone, siltstone, and mudstone, and interbedded tuffaceous mudstone are also observed.

The XRD analysis of samples from the tuff interval shows that the clay mineral content is mainly distributed between 20% and 50%, the carbonate mineral content is mainly >50%, and the content of quartz and feldspar is typically <20% (Fig. 4). The other components include rhodochrosite, magnesite, pyrite, galena, barite, and common pyroxene. Glass and crystal debris are observed under a microscope. Glass shards are sharp, irregular, cambered, and angular in shape. The lava is composed mostly of rhyolite and andesite. The glass debris is primarily composed of quartz, feldspar, and glass.

4.2. Organic-inorganic geochemical characteristics

Among the 11 samples of Well Fu117 tested, TOC is 0.23%–5.08% (average = 2.20%), S_1+S_2 is 0.28–26.29 mg/g (average = 10.75 mg/g), and T_{max} is 445.00–453.00 °C (average = 449.27 °C). Among the eight samples of Well QD25 tested, TOC is 1.19%–5.38% (average = 2.60%), S_1+S_2 is 0.25–10.28 mg/g (average = 3.95 mg/g), T_{max} is 361.00–443.00 °C (average = 424.83 °C) (Fig. 5).

The oil-bearing tuffaceous shale interval is characterised by a negative spontaneous potential, well diameter expansion, large number of natural gamma abrupt intervals, and low resistivity value (RLLD < 60). The interval transition time, neutron porosity,

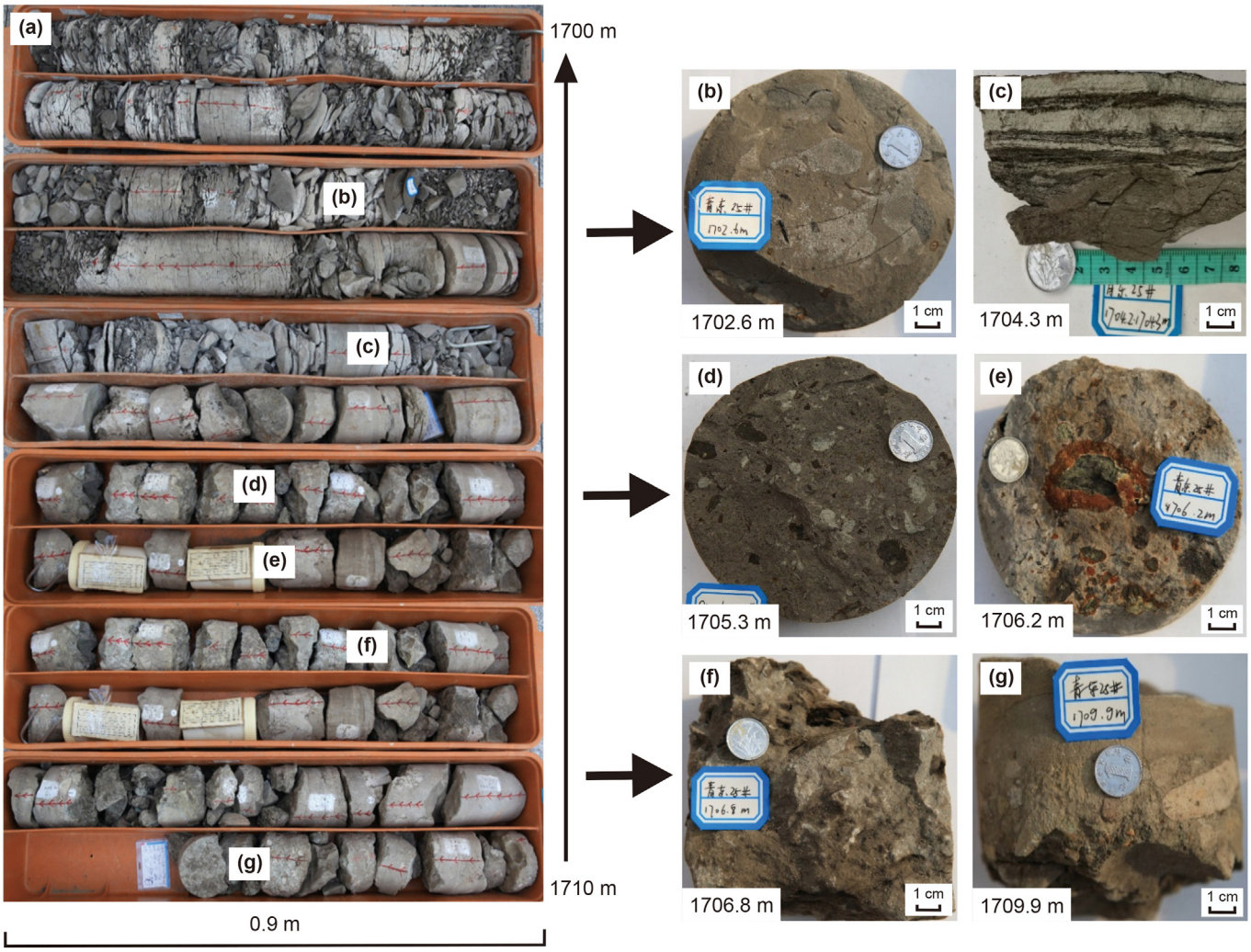

Fig. 2. Tuff shale section core from the Es_4^1 of the shale samples of Well QD25: **(a)** At a depth of 1700–1710 m of the Well QD25, there are positive grain order features, transitioning from tuffaceous conglomerate **(f, g)** to fine tuffaceous sandstone **(d, e)**, and finally to tuffaceous shale and shale **(b, c)**.

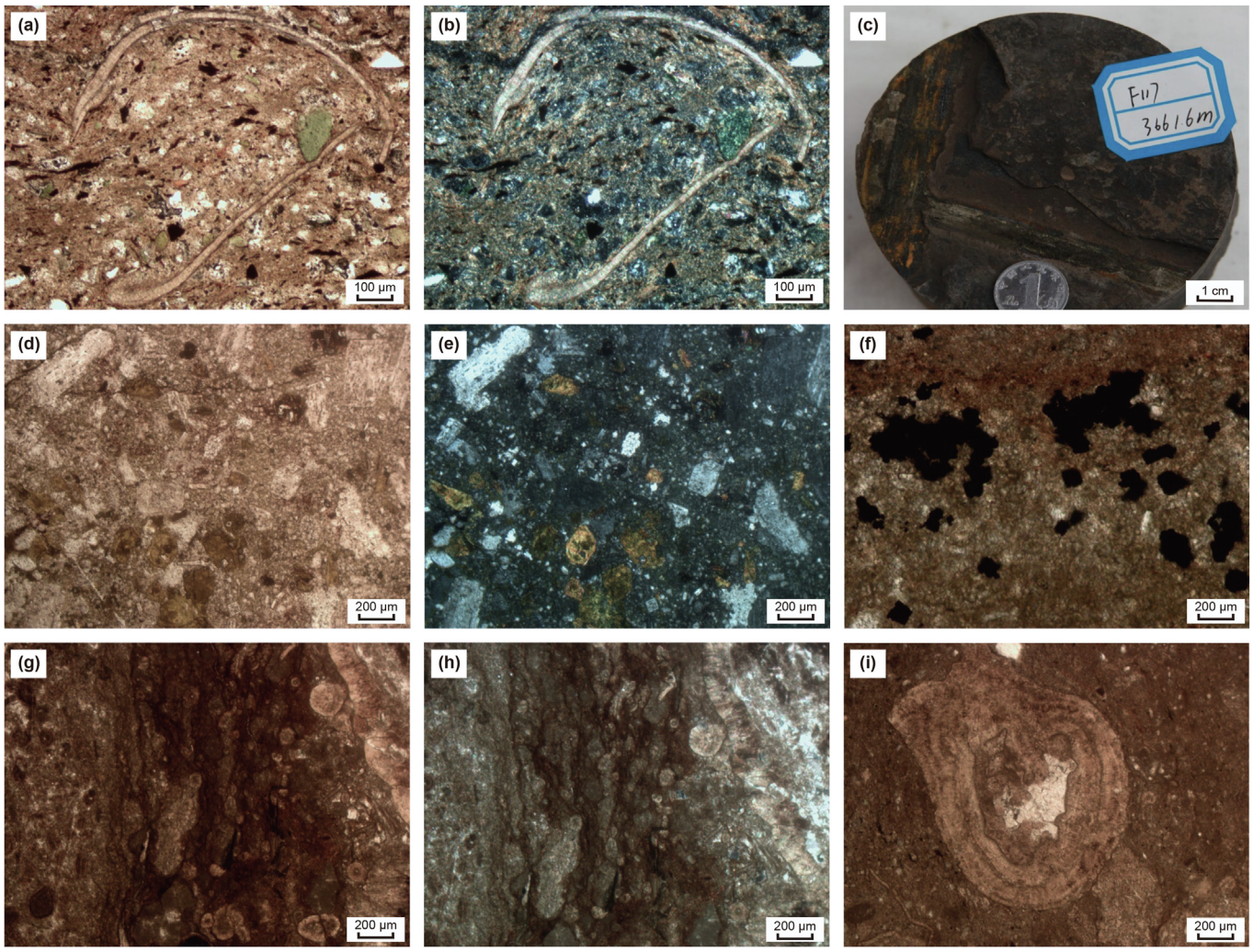

Fig. 3. Biological heritage of the Es_4^1 and Es_3^3 shale samples. **(a, b)** Organic texture under the microscope: **(a)** plain polarised light, **(b)** cross-polarised light; it is accounted for by calcite (QD25-3). **(c)** The plant fossils (Fu117-6). **(d, e)** Andesite with a banded structure developed with basic plagioclase, and the glassy is being devitrified: **(d)** plain polarised light, **(e)** cross-polarised light (Fu117-15). **(f)** Pyrite with a particle size of 20–80 μm (Fu120-1). **(g, h, i)** The layered algal fossils: **(g)** plain polarised light, **(h)** cross-polarised light, and **(i)** the close-up of algal fossil (Fu117-11).

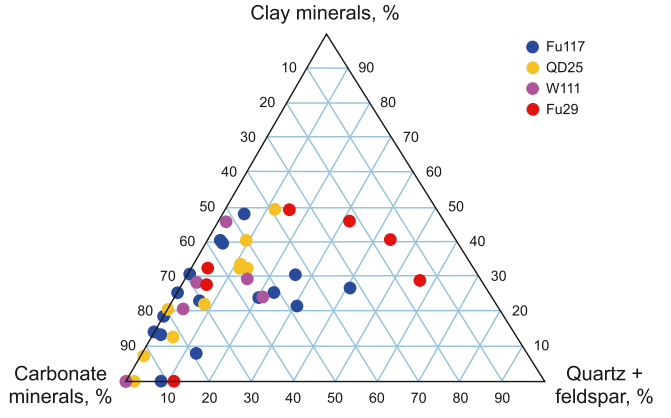

Fig. 4. Whole rock mineral analysis results of the organic-rich shales from Es_4^1 and Es_3^3 samples. The clay mineral content of the samples is mainly distributed between 20% and 50%, the carbonate mineral content is mainly >50%, and the quartz + feldspar content is <20%.

density, and resistivity curves of the oil-bearing tuffaceous shale intervals are mostly box-shaped with evident curve changes, and abrupt changes in magnetic susceptibility locally. The magnetisation rate of tuffaceous mudstone is higher than that of shales without tuff, and the TOC and hydrogen index (HI) of mudstone between tuffaceous mudstones are also high (Fig. 5).

XRF analysis of the major elements reveals that the SiO_2 content of most tuffaceous shale intervals from the Shahejie Formation in the Jiyang Depression is 28.22%–69.43%, the CaO content is 0.49%–41.85%, and the Al_2O_3 content is 2.54%–16.71%, followed by Fe_2O_3, MgO, and K_2O (Table 1). The chemical composition of the tuffaceous interval (1701–1710 m) in well QD25 is dominated by SiO_2 and Al_2O_3 with contents ranging from 10% to 60% and 10%–22%, respectively. The contents of Fe_2O_3 and sulphur have maxima of 19.80% and 20.60% (average = 4.16% and 5.25%), respectively. There is a low content of P_2O_5, K_2O, MgO, CaO, TiO_2, and MnO. The main trace elements with higher contents are V, Cu, Zn, Ba, Rb, Sr, Y, and Mo, which are iron-philic and sulphur-philic elements (Fig. 6). The elemental contents of samples from well Fu117 are similar to those

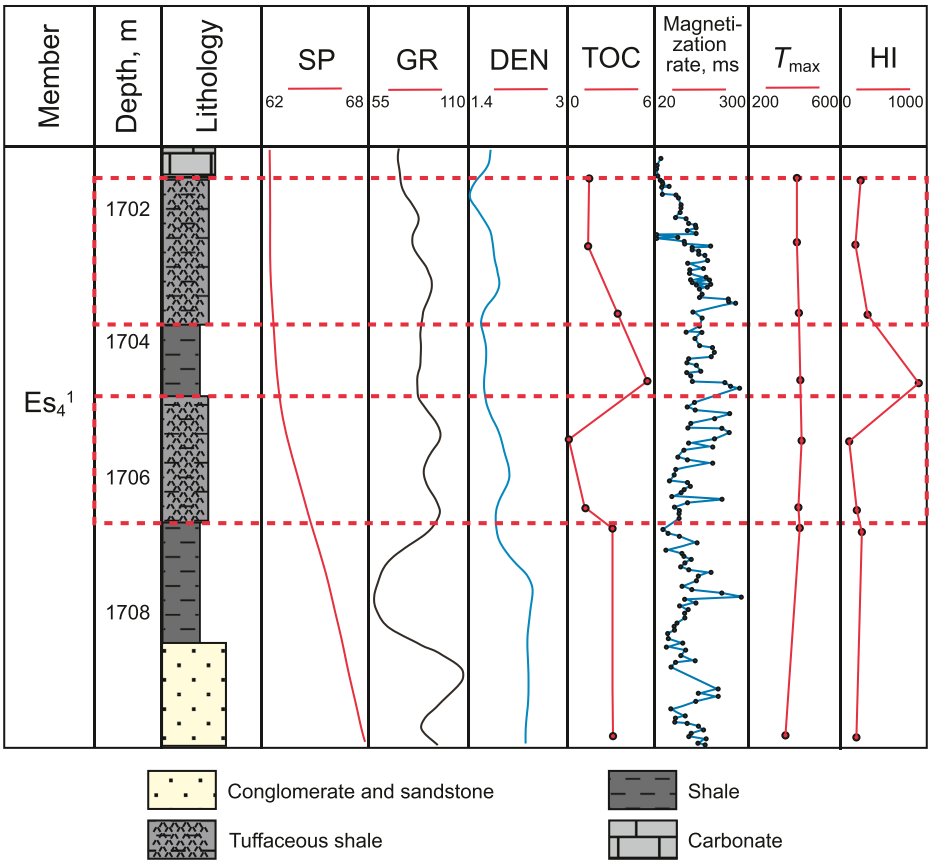

Fig. 5. Log of lithology, self-potential logging (SP), gamma-ray logging (GR), density logging (DEN), TOC, magnetic susceptibility, hydrogen index (HI), and T_{max} from 1701 to 1710 m in Well QD25. The magnetic susceptibility of tuffaceous mudstone is higher, and the TOC and HI of mudstone between tuffaceous mudstones is higher.

Table 1
Major elements found in Fu117 and QD25 samples.

Samples	Depth, m	Na_2O, %	MgO, %	Al_2O_3, %	SiO_2, %	P_2O_5, %	K_2O, %	CaO, %	TiO_2, %	MnO, %	Fe_2O_3, %	LOI, %
Fu117-3	3661.00	0.76	6.97	9.67	35.23	0.59	2.37	15.44	0.52	0.16	4.49	23.81
Fu117-4	3661.30	1.16	2.52	14.70	52.12	0.48	3.60	8.13	0.87	0.07	3.71	12.64
Fu117-5	3661.40	1.21	2.27	13.82	54.32	1.18	3.08	4.85	0.81	0.04	4.64	13.79
Fu117-6	3661.60	0.53	2.68	10.09	32.60	1.03	2.48	20.00	0.58	0.12	4.71	25.19
Fu117-7	3661.80	0.87	4.43	10.75	44.51	0.61	2.49	9.23	0.59	0.13	7.33	19.07
Fu117-8	3664.50	1.03	2.51	14.40	49.39	0.46	3.49	10.16	0.94	0.08	3.73	13.83
Fu117-9	3664.80	0.88	3.02	14.94	54.21	0.48	3.70	5.52	0.87	0.05	2.98	13.35
Fu117-10	3665.10	1.63	1.90	12.68	56.20	0.42	2.99	4.74	0.73	0.04	6.32	12.36
Fu117-12	3665.40	0.79	2.88	11.29	45.96	0.34	2.61	12.58	0.68	0.10	4.95	17.84
Fu117-11	3665.70	0.49	3.47	9.40	34.22	0.54	2.43	21.77	0.64	0.10	3.34	23.59
Fu117-13	3666.00	0.25	2.99	2.54	12.69	0.30	0.59	41.85	0.14	0.17	1.70	36.79
QD25-1	1701.50	0.86	2.01	15.50	50.24	0.40	4.45	5.62	0.71	0.05	7.13	13.03
QD25-2	1702.60	1.10	1.98	15.72	53.50	0.33	4.64	3.82	0.70	0.04	6.86	11.31
QD25-3	1703.20	0.78	2.16	16.17	50.62	0.29	4.87	4.46	0.72	0.04	6.96	12.94
QD25-4	1704.20	1.74	1.42	12.51	56.29	0.24	3.75	6.56	0.51	0.15	4.97	11.86
QD25-5	1704.30	0.88	1.83	15.26	52.86	0.44	4.88	4.49	0.65	0.04	6.22	12.45
QD25-12	1705.30	1.11	1.70	14.67	56.13	0.37	4.86	3.32	0.62	0.03	6.29	10.89
QD25-6	1705.40	1.05	1.80	14.99	56.18	0.41	5.03	2.63	0.67	0.03	6.27	10.94
QD25-7	1705.50	0.76	2.19	16.71	53.22	0.21	5.28	1.54	0.73	0.03	6.68	12.66
QD25-8	1705.80	1.77	1.00	12.03	68.73	0.36	4.31	1.35	0.41	0.03	3.80	6.23
QD25-9	1706.20	0.99	0.31	5.34	30.97	0.39	1.75	32.63	0.17	0.19	3.08	24.19
QD25-10	1706.80	1.88	0.48	9.81	45.23	0.16	2.72	19.89	0.20	0.22	2.20	17.21
QD25-13	1709.10	2.29	0.83	12.59	69.43	0.15	4.59	0.49	0.48	0.02	2.58	6.55
QD25-11	1709.90	1.82	2.15	14.73	61.50	0.25	4.57	0.64	0.66	0.04	5.85	7.79

of samples from well QD25. The contents of SiO_2 are between 10% and 63.3% and the Al_2O_3 content is 15.40%. The Fe_2O_3 content in the sample from well QD25 reaches 53.30%, whereas the S content is only 2.40%. In addition, the P_2O_5, K_2O, MgO, CaO, TiO_2, and MnO contents are low in all samples. The ICP-MS results show that the tuff layer samples are rich in LREE with moderate Eu anomalies represented by $(La/Yb)_{PAAS}$ = 1.4–3.4 (average = 2.28) and Eu* PAAS = $2(Eu)_{PAAS}/(Sm + Gd)_{PAAS}$ = 1.15–1.67 (average = 1.32)

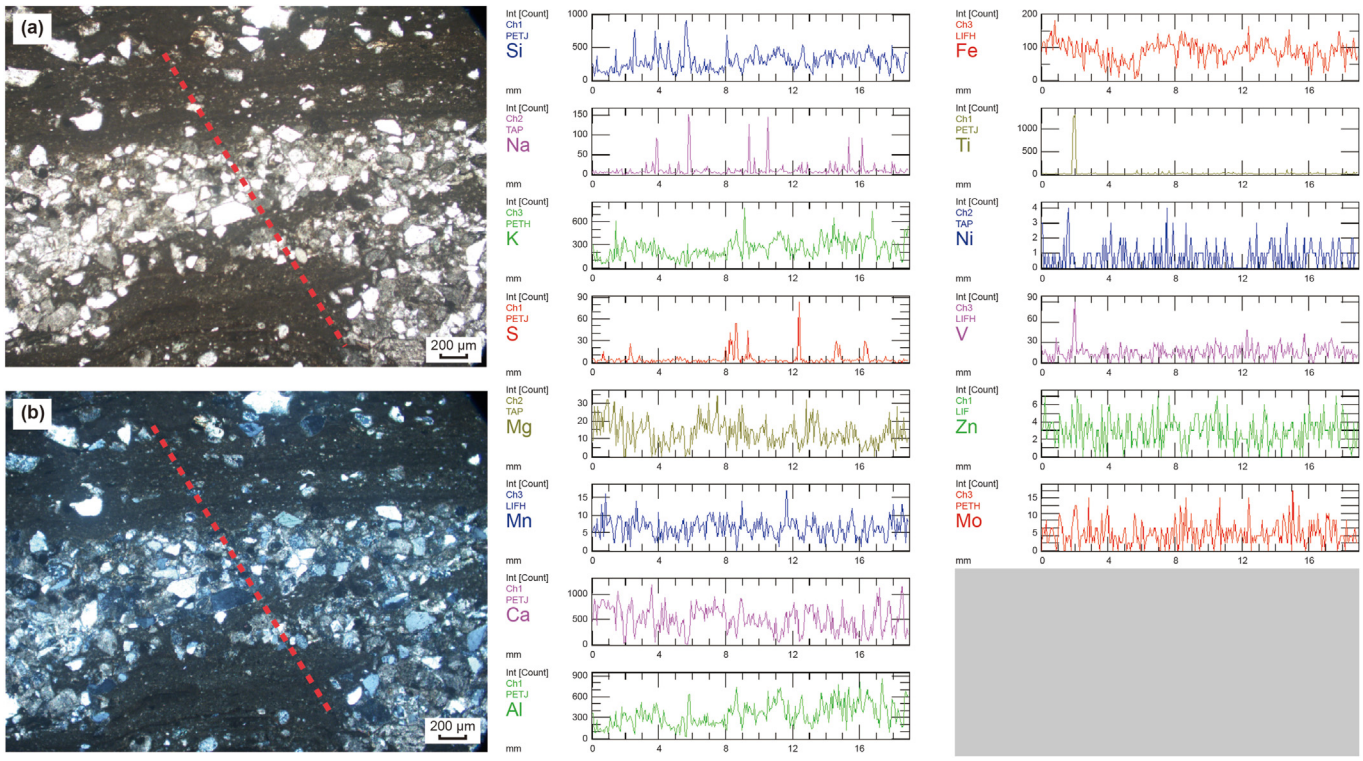

Fig. 6. Elemental content of tuff samples from Es_4^1 and Es_3^3 shale samples. **(a)** Volcanic material under the microscope (plain polarised light). **(b)** The quartz grain lens with a high degree of automorphism is surrounded by clay minerals (cross-polarised light). The elemental content is measured along the dotted red lines in **(a)** and **(b)**. These quartzes are carried by volcanic ash. As the ash descends from the atmosphere, the quartz is deposited directly into the water column. As the elemental content plot shows, the quartz, located in the middle of the measured red dashed line, has more sulphur.

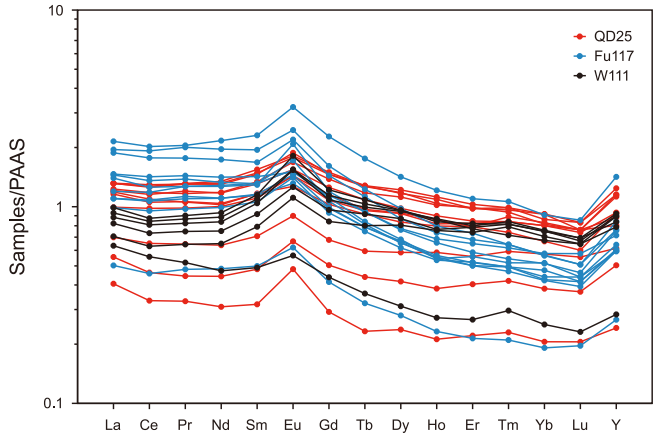

Fig. 7. Rare earth element (REE) distribution pattern in Es_4^1 and Es_3^3 shale samples in Wells QD25, Fu117, and W111 (The Post Archean Australian average shale (PAAS) data are from Taylor and Mclennan, 1985.)

(superscript * denotes the anomalies, subscript PAAS denotes the Post Archean Australian average shale) (Fig. 7).

5. Discussion

5.1. Volcanic impact on the formation of organic-rich shale

In the study area, volcanic ash is mainly developed via hydrodynamic genesis and slightly differs from that associated with airborne genesis. Generally, tuff interlayers are developed with occasional crumpling and slumping of sandstone and mudstone, sometimes even enveloped the bedding and cross-bedding synsedimentary structures (Fig. 2). This phenomenon shows that the tuff formation in the study area is a water-carrying type and might be accompanied by strong tectonic activity (Wang et al., 2003). This may be the reason for the gravity sliding that occurred in sand and mudstone under certain triggering conditions, such as slumps, debris flows, and turbidites, leading to the redeposition of these sediments (Wang et al., 2003).

Based on our core observations, tuff interlayers demonstrate a distinct distribution pattern within the Jiyang Depression. These interlayers are primarily concentrated in two key regions: the central basin and areas adjacent to fault lines. In order to gain a better understanding of these tuff interlayers, it is crucial to differentiate between their genetic types in different geological settings. In deep lake environments, such as Well FY1, the predominant genetic type of tuff interlayers is of the airborne nature. These tuff layers are located far from the centre of volcanic eruptions, as volcanic ash can be transported long distances by wind. When analysing the sedimentary structure of these airborne tuff interlayers, they are observed to be connected with both upper and lower shale formations. However, their occurrence is relatively restricted within other sedimentary structures. In the Dongying Sag, specifically at Well FY1, we observe tuffaceous shale formations at a depth of 3208 m. These tuffaceous shales are predominantly present in layered and laminated intervals of organic-rich shale. These intervals are distinguished by their relatively pure composition and thinness. In contrast, tuff interlayers found in semi-deep lakes and nearshore underwater fans are primarily formed by water. These water-carrying tuffs have similar sedimentary structures to clastic rocks. They have a higher clastic composition and often contain hydrolytic alteration minerals.

However, they show less regional consistency. Within the Fulin sub-sag of the Qingdong and Zhanhua sags, the strata containing tuffaceous intervals exhibit a relatively loose texture but display rhythmic bedding. These strata consist of pyroclastics with varying particle sizes, and a discernible pattern can be observed with coarser layers positioned below and finer layers positioned above. The transition sequence in this area is primarily characterised by tuffaceous glutenite, tuffaceous siltstone, tuffaceous and argillaceous interbeds, and pure tuff.

The total amount of trace elements significantly increased in the layered-laminated organic-rich shale of Well FY1, such as rare earth elements (REEs). This may reflect a sudden change in the composition of the water body. Here, we propose that the volcanic ash carried sufficient nutrients and trace elements, such as Mo (Fig. 8(a)), Fe (Fig. 8(b)), Ni (Fig. 8(c)), and Zn (Fig. 8(d)), that promoted the growth of organisms under suitable temperature conditions in the basin (Liu et al., 2019). After a large amount of oxygen is consumed, an oxygen-deficient environment was formed, leading to the death of the organisms. Thus, the rich OM is effectively preserved. High primary paleoproductivity, deep hydrothermal activity, and volcanic eruptions created an anoxic environment favourable for the burial and preservation of OM (Fig. 8(e)) (Liu et al., 2018). The under-compensated environment in the centre of the lacustrine basin promoted the enrichment of OM. All these conditions created favourable conditions for the formation of high-quality source rocks (Fig. 9) (Liu et al., 2022a, 2022c; Xie et al., 2023).

In summary, volcanism, whether occurring at the margins or

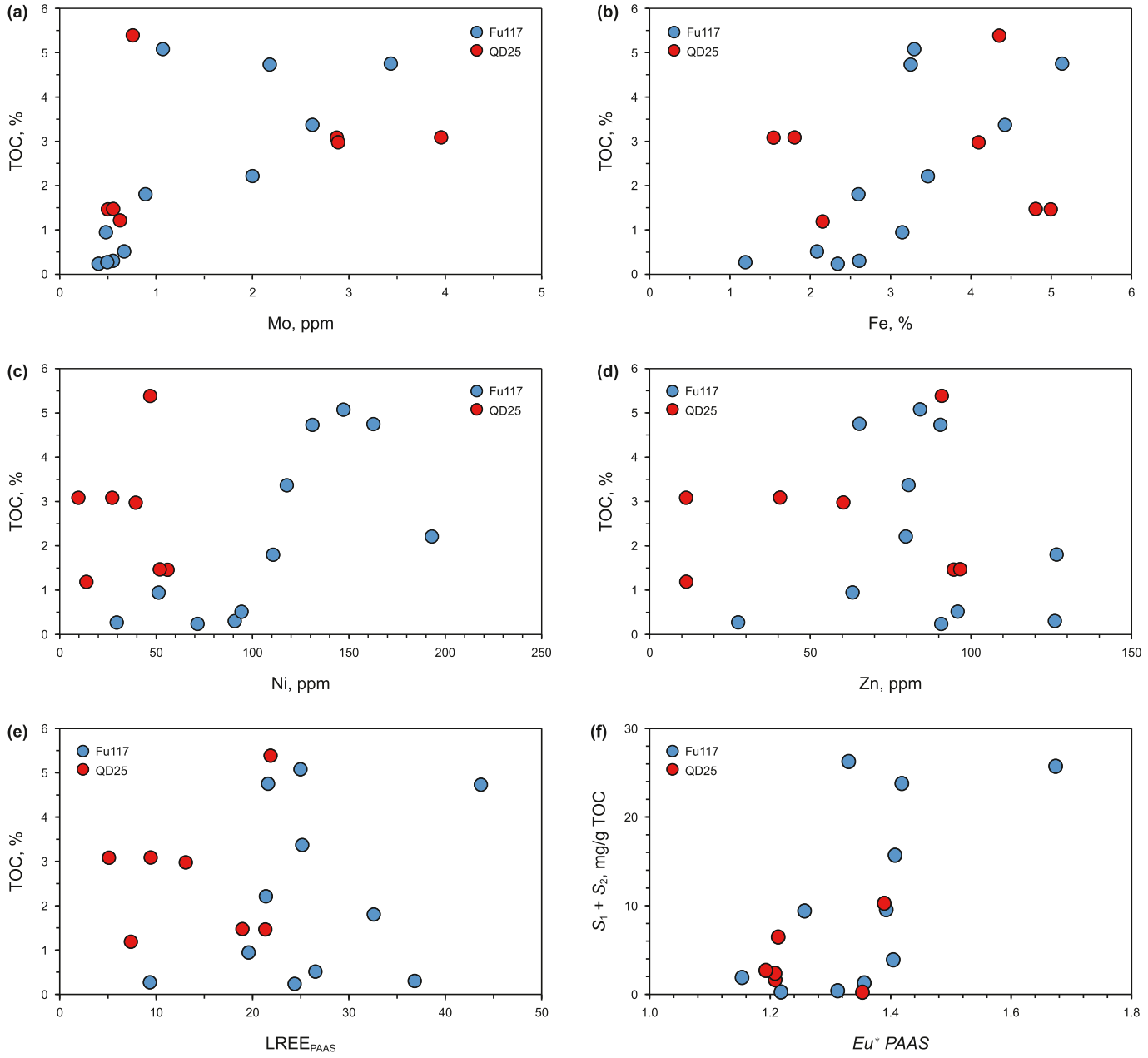

Fig. 8. Relationship between TOC and trace elements. **(a)** TOC-Mo, **(b)** TOC-Fe, **(c)** TOC-Ni, and **(d)** TOC-Zn in Es_4^1 and Es_3^3 of the Shahejie Formation shale samples from Wells QD25 and Fu117. **(e)** The TOC and $LREE_{PAAS}$ cross-plot show that moderate amounts of LREE have a positive impact on the formation of OM $LREE_{PAAS}$. **(f)** The S_1+S_2 and Eu* PAAS cross-plot shows that hydrothermal fluid activity may increase the intensity of hydrocarbon generation.

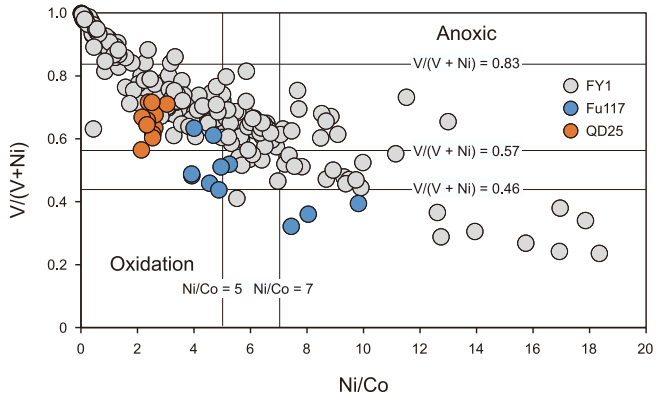

Fig. 9. Ni/Co and V/(V + Ni) cross-plot shows that the depositional environment is anoxic during the Es_4^1 and Es_3^3 of the Jiyang Depression. When the Ni/Co < 5, it indicates an oxic environment; when the Ni/Co > 7, it indicates an anoxic environment; and 5 < Ni/Co < 7 indicates a sub-oxygenic environment (Jones and Manning, 1994). When the V/(V + Ni) > 0.83, it indicates a static sea environment; between 0.57 < V/(V + Ni) < 0.83, it indicates an anoxic environment; between 0.46 < V/(V + Ni) < 0.57, it indicates a weak oxidizing environment; and V/(V + Ni) < 0.46 indicates an oxidizing environment (Hatch and Leventhal, 1992).

within the confines of a basin, introduces significant quantities of nutrient-enriched volcanic ash into the water body. This influx of nutrients results in an enhanced proliferation of algae, indicating a rise in paleoproductivity attributed to volcanism. Over time, this burgeoning algal population depletes oxygen reserves. Concurrently, the volcanic ash, which is rich in sulphur, promotes the development of a reducing environment within the basin (Liu et al., 2022a, 2022b, 2022c). Such conditions are favourable for the burial and subsequent preservation of organic matter (OM). In this study, we indicate positive facilitation of the volcanic impact on the formation and preservation of organic-rich shales in the Jiyang Depression. However, our study only qualitatively describes the impact of volcanic activity on the formation of organic-rich shale in the Shahejie Formation in the Jiyang depression. Since the thickness of the ash in the shale is a proxy for the eruption's strength, future research under the conditions satisfied by core samples for the shale oil/gas sweet spot evaluation and prediction can be quantitative and more comparative.

5.2. Influence of volcanism on hydrocarbon generation in organic-rich shale

The impact of volcanism on the hydrocarbon generation intensity of the OM mainly depends on the heat directly brought about by magma intrusion which promotes OM evolution. The imported trace elements and clay minerals produced by the devitrification of volcanic materials also act as catalysts for the evolution of OM (Fisher and Schmincke, 1984; Huff, 2016). Here, we propose a possible catalysis caused by volcanic activity during the formation of organic-rich shales in the Jiyang Depression and discuss the influence of volcanic activity on hydrocarbon generation using the Qingdong Sag as an example.

5.2.1. Catalytic effect of volcanism

Thermocatalysis. Sediment enters the early diagenesis stage when its burial depth exceeds 1500 m (Guo et al., 2018, 2020). The temperature experienced by the OM in the sediments rose from 60 °C to 180 °C (Bian et al., 2015; Wang et al., 2016). If the sediments contain volcanic substances, a greater amount of radioactive elements (such as Th, Zr, Hf, and U) increase the formation temperature, as radioactive elements release heat during decay (Liang et al., 2021). An increase in the ground temperature facilitates the maturation of OM. As a result, the decay heat release of radioactive elements in volcanic substances plays an important role in promoting hydrocarbon generation and the evolution of source rocks and increasing the hydrocarbon generation intensity in organic-rich matter (Liang et al., 2021; Liu et al., 2021). Additionally, the shallow intrusion by magma increases the temperature of organic-rich shale, affecting the evolution of OM. The positive correlation between S_1+S_2 and Eu* PAAS indicates hydrothermal activities might have promoted OM hydrocarbon generation (Fig. 8(f)).

Catalysis of trace elements. Large amounts of catalytic elements imported into the basin by volcanism facilitate hydrocarbon generation from OM. The Mo and Zn significantly promoted the degradation of organic matter (Fig. 10). Transition metals, as well as their oxides, sulphides, and other derivatives, have significant catalytic effects on hydrocarbon generation by organic compounds (Liang et al., 2021). It has been widely used in oil refinery cracking and chemical industry of refineries (Trowbridge et al., 2020). Volcanic ash formation is typically accompanied by magmatic activity and hydrothermal eruptions. In addition, it carries large amounts of high-temperature and high-pressure mantle hydrothermal fluids and various metal elements such as Fe, Cu, Zn, and Ag (Duggen et al., 2007; Liang et al., 2021; Liu et al., 2021). Volcanism also carries typical trace catalytic elements, such as Se, Zr, Ti, V, Co, Mn, Ni, Mo, and U, which promote the thermal evolution of hydrocarbon generation in source rocks (Liang et al., 2021; Liu et al., 2021). Most transition-metal oxides exhibit catalytic activities, such as semiconductivity, and acid–base and redox properties, under different acid–base conditions. Studies have shown that among transition metals, Ni has the strongest catalytic performance (Su et al., 2015). The Ni content in the source rock is 1×10^{-6}, which indicates strong catalytic power (Su et al., 2015). Ni can adsorb gases and OM, breaking its C–C, C–S, and C–O bonds, thereby achieving catalysis (Su et al., 2015). Therefore, the trace elements carried by volcanic materials have a significant catalytic hydrocarbon-enhancing effect.

Catalysis of clay minerals. Strata affected by volcanism contain materials that can be altered into clay through debasement (He et al., 2001; Fang, 2016; Jin et al., 2021). The transformation of volcanic materials into clay minerals is important for generating OM hydrocarbons. Clay minerals (such as illite and montmorillonite) produced via tuff alteration may also play an important catalytic role in the source rocks (Hong et al., 2019a; 2019b). Clay minerals often adsorb radioactive elements, and bombardment with the alpha rays emitted by radioactive elements generates large amounts of free hydrogen (Yu et al., 2014; Zeng et al., 2016; Tian et al., 2020). The combination of free hydrogen and carbon generates hydrocarbons. Therefore, the alpha rays emitted by these radioactive substances may supply the thermal power necessary for converting OM into hydrocarbons.

Previous studies (Lin et al., 2003; Xu et al., 2019; Liu et al., 2022a, 2022c) have analysed the formation of organic-rich shales in the Shahejie Formation based on the astronomical cycle, climate change, regional tectonic thermal events in the geothermal field of the basin, and the relationship between oil and gas accumulation laws (Xu et al., 2019; Liu et al., 2022a, 2022c). Few studies have been conducted on the petrography of sediments in the basin (particularly tuff and its alteration products), diagenetic changes, the influence of sediments on the geothermal temperature of the basin, and the evolution of source rocks. The alteration products of the tuff are mainly clay minerals (the main body is an I-Mont mixed layer). Clay minerals have significant catalytic effects on OM (Pearson et al., 2002; Jin et al., 2021). In this study, we propose that the clay minerals transferred by tuff reduce the maturation temperature of OM and promote hydrocarbon generation. The chemical

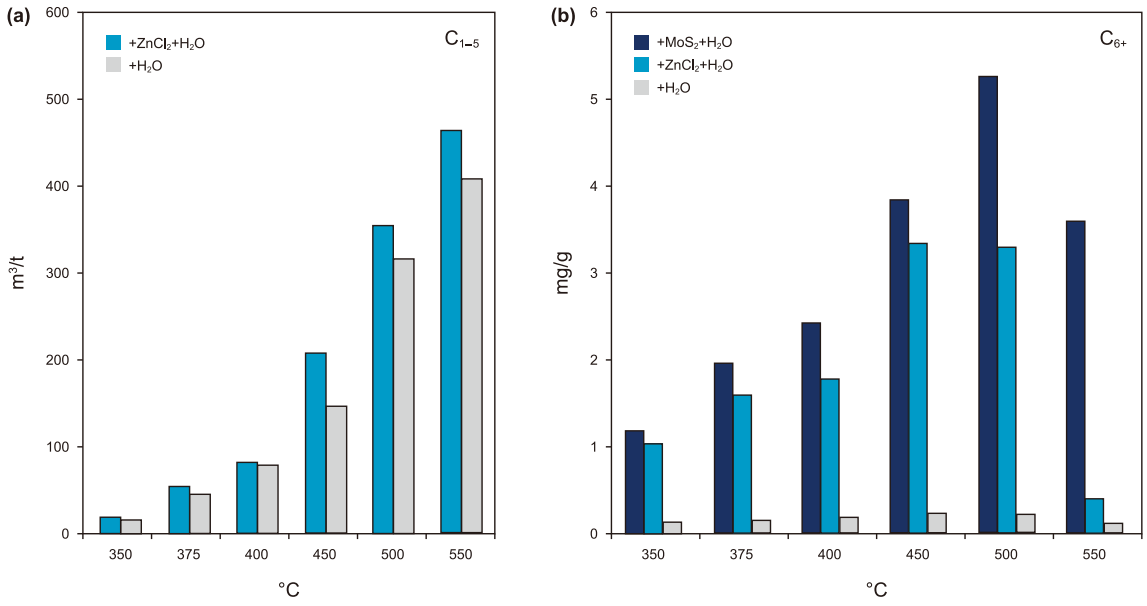

Fig. 10. Experimental study on the effect of trace elements on kerogen hydrocarbon generation. **(a)** The effect of Zn on the generation of C_{1-5}. **(b)** The effect of Zn and Mo on the generation of C_{6+}.

composition and yield of kerogen pyrolysis hydrocarbons are also affected by clay minerals. The catalysis of clay minerals not only cracks long-chain hydrocarbons into short-chain hydrocarbons, but also relatively decreases the content of olefins and relatively increases the contents of isoparaffins, naphthenes, and aromatic hydrocarbons. The strengths of the catalysis, adsorption, and coking of different clay minerals and OM differ. The most common product of volcanic ash alteration is montmorillonite, which has the greatest influence on the composition of kerogen pyrolysis hydrocarbons. This indicates that tuff has a catalytic effect on organic hydrocarbon generation. Among the four different sub-depressions in the Huimin Depression, strong volcanic activity and deep fluids are detected, which carried high heat and maintained the high ground temperature over a long period. In addition, the external hydrogen source resulting from secondary action and volcanic ash compensated for the lack of shallow burial. OM begins to generate hydrocarbons before reaching the normal oil generation threshold. Consequently, the overall maturity of the Huimin Depression is relatively high.

5.2.2. A case study of the volcanic influence on hydrocarbon generation in Qingdong Sag

Well QD25 is located in the northwestern area of the Qingdong Sag, close to the deep faults in the basin. Based on the distribution map of the hydrocarbon generation intensity in Es_4^1, the S_1+S_2 value of this well during this period is higher than that of adjacent areas. The hydrocarbon generation intensity of this well is also higher than that of the other adjoining well areas during the diagenetic stage. During the depositional period of Es_4^1, the Qingdong Sag is dominated by shallow coastal and semi-deep lakes, with deep depressions in the north and shallow lakes in the south (Li et al., 2009; Jia et al., 2019). The sag mainly developed deep-to-semi-deep lacustrine deposits that significantly controlled the development of OM in these depressions (Ma, 2014). Although QD25 is far from the depositional centre, Es_4^1 of QD25 has a higher hydrocarbon generation intensity than the surrounding area, which is likely due to volcanism. Core observations showed 10 m of volcanic material deposits in 1701–1710 m in the upper part of Es_4^1. The lithologies and particle sizes are different, and tuffaceous sandstone, siltstone, and shale are presumed to be water-carrying tuffs. This implies that volcanism is one of the reasons for the high hydrocarbon generation intensity in QD25 (Fig. 11). To discuss the influence of volcanism on hydrocarbon generation in organic-rich shale, three contour maps of TOC, R_o, and S_1+S_2 were superimposed to explain the phenomenon that QD25 well is located at the edge of the basin; however, its hydrocarbon generation intensity is still high as the result of volcanic impact. Fig. 11 shows that QD25 is located near the first level fault, far from the sedimentary centre, with lower TOC and R_o, but higher S_1+S_2, which may be caused by the baking of adjacent strata by magma after volcanism. Areas that are far from the centre of the basin and have lower TOC may be affected by volcanism and have higher hydrocarbon generation intensity, such as the QD11 and QD30 well.

The different geneses of the tuffs may be the reason for the different intensities of OM hydrocarbon generation. The types of volcanic ash in Es_4^1 are airborne. Previous studies have shown that the R_o of dark mudstone in Es_4^1 of the Qingdong Sag is 0.32%–0.51% (average = 0.46%), which is immature to low-maturity source rock, and the types of volcanic ash in Es_3^3 are waterborne. The R_o of the dark mudstone in Es_3^3 of the Qingdong Sag had a range of 0.32%–0.52% (average = 0.44%). It is an immature–low-maturity source rock (Liu, 2016).

6. Conclusions

There is a temporal hysteresis in the response of the volcanic impact to the formation of organic-rich shale. Comprehensive sedimentary and geochemical analyses showed that the nutrients (such as Fe, Cu, and Ni) carried by volcanic ash improved primary productivity and promoted biological blooms during the deposition of Es_4^1 and Es_3^3 in the Jiyang Depression. Biological blooms then consumed large amounts of oxygen and formed anoxic environments, which are conducive to the burial and preservation of OM in Es_4^1 and Es_3^3. Therefore, a lower TOC value is observed in the tuff intervals than in the upper shale interlayers. In addition, volcanism promotes hydrocarbon generation of OM. The different geneses of volcanism may be the reason for the thermocatalysis and catalysis of trace or clay mineral intensities in OM hydrocarbon generation.

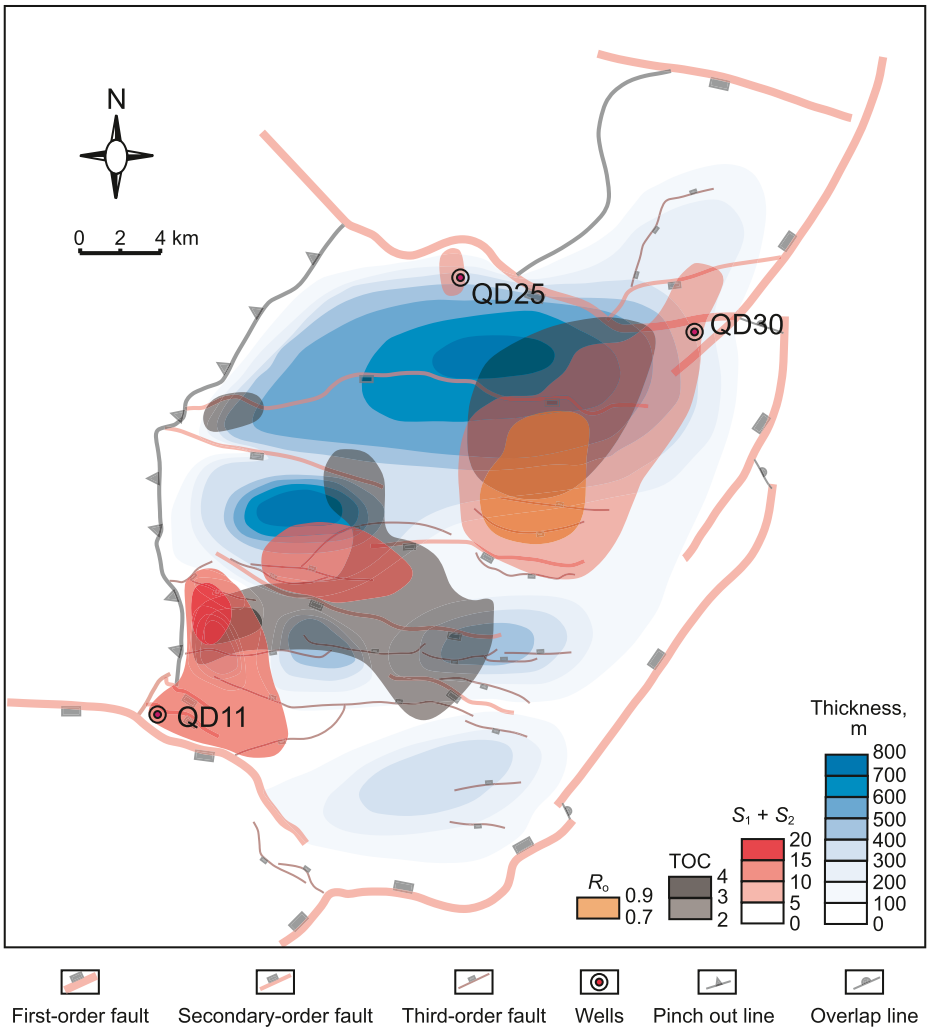

Fig. 11. Congruent figures of TOC, R_o, and $S_1 + S_2$ values from Es_4^1 shale samples in the Qingdong Sag (Modified from Liu, 2016). This picture is adapted from the shale thickness, TOC, R_o, and $S_1 + S_2$ contour map of Es_4^1 in Qingdong Sag by Liu (2016).

Further studies are required to quantitatively evaluate the catalytic effects on hydrocarbon generation in organic-rich shales.

Volcanic activity is a manifestation of deep fluids, and deep fluids are widely developed not only in the Jiyang Depression but also in other lacustrine and marine basins. Further research is suggested to focus on the materials and energy carried by deep fluids, explore the enrichment mechanism of OM, the hydrocarbon evolution of source rocks, and the conducive conditions for the formation of reservoirs and caprocks under deep geological processes. It is also recommended to establish the geochemical tracer index system of formation, migration, and accumulation in deep oil and gas under the effect of deep fluids. Further research is needed to clarify the influence mechanism of deep fluids on the formation and distribution of multiple types of resources in sedimentary basins, clarify the resource accumulation effect and resource potential of materials and energy carried by them, and then reveal the controlling factors of differences in different regions. Research in these aspects not only enriches and improves the theoretical system of formation of oil, gas and geothermal resources in basins but also provides a scientific basis and guiding ideas for the discovery, efficient development, and utilisation of new resources.

Declaration of competing interest

The authors declare that they have no known competing financial interests or personal relationships that could have appeared to influence the work reported in this paper.

Acknowledgements and Funding

The authors thank Ming-Shui Song, Shao-Quan Tan, and Dong Guo for their help with samples collection; Yun-Qing Hao with microscopic slice analyses and useful discussions; and the China University of Geology (Wuhan) for all geochemical analyses. We acknowledge the financial support from the National Natural Science Foundation of China (42172151, 42090025, 41811530094, and 41625009), the China Postdoctoral Science Foundation (2021M690204), and the National Key Research and Development Program (2019YFA0708504 & 2023YFF0806200). We thank the anonymous reviewers for their constructive comments, which have greatly improved the quality of this paper.

Abbreviations

Es_4^1	the upper submember of the fourth member of Shahejie Formation
Es_3^3	the lower submember of the third member of Shahejie Formation
REEs	rare earth elements
LREE	light rare earth elements
R_o	the vitrinite reflectance, which is considered an important index reflecting the thermoevolution history of organic materials
S_1+S_2	hydrocarbon-generating intensity
OM	organic matter
TOC	total organic carbon
XRD	X-ray diffraction
XRF	X-ray fluorescence
ICP-MS	inductively coupled plasma mass spectrometry
PAAS	Post-Archean Australian Shale

References

Batchelor, R.A., 2003. Geochemistry of biotite in metabentonites as an age discriminant, indicator of regional magma sources and potential correlating tool. Mineral. Mag. 67, 807–817. https://doi.org/10.1180/0026461036740137.

Bian, C.S., Zhao, W.Z., Wang, H.J., Chen, Z.Y., Wang, Z.C., Liu, G.D., Zhao, C.Y., Wang, Y.P., Xu, Z.H., Li, Y.X., Jiang, L., 2015. Contribution of moderate overall coal-bearing Basin uplift to tight sand gas accumulation: case study of the Xujiahe formation in the Sichuan Basin and the upper Paleozoic in the Ordos Basin, China. Petrol. Sci. 12, 218–231. https://doi.org/10.1007/s12182-015-0030-0.

Dennison, J.M., Textoris, D.A., 1970. Devonian tioga tuff in Northeastern United States. Bull. Volcanol. 34, 289–294. https://doi.org/10.1007/BF02597791.

Demaison, G.J., Moore, G.T., 1980. Anoxic environments and oil source bed genesis. Org. Geochem. 2, 9–31. https://doi.org/10.1016/0146-6380(80)90017-0.

Dick, G.J., Anantharaman, K., Baker, B.J., Li, M., Reed, D.C., Sheik, C.S., 2013. The microbiology of deep-sea hydrothermal vent plumes: ecological and biogeographic linkages to seafloor and water column habitats. Front. Microbiol. 4, 124. https://doi.org/10.3389/fmicb.2013.00124.

Diego, A.K., Ricardo, M.P., Alberto, C.R., Javier, M.C., Jose, L.G., 2014. Sedimentology and sequence stratigraphy of a Tithonian–Valanginian carbonate ramp (Vaca Muerta formation): a misunderstood exceptional source rock in the southern Mendoza area of the Neuquén Basin. Argentina. Sediment. Geol. 302, 64–86. https://doi.org/10.1016/j.sedgeo.2014.01.002.

Du, J.H., Mix, A.C., Haley, B.A., Belanger, C.L., Sharon, 2022. Volcanic trigger of ocean deoxygenation during Cordilleran ice sheet retreat. Nature (London) 611, 74–80. https://doi.org/10.1038/s41586-022-05267-y.

Duggen, S., Croot, P., Schacht, U., Hoffmann, L., 2007. Subduction zone volcanic ash can fertilize the surface ocean and stimulate phytoplankton growth, evidence from biogeochemical experiments and satellite data. Geophys. Res. Lett. 34, L01612. https://doi.org/10.1029/2006GL027522.

Edmonds, M., Mason, E., Hogg, O., 2022. Volcanic outgassing of volatile trace metals. Annu. Rev. Earth Planet Sci. 50, 79–98. https://doi.org/10.1146/annu-rev-earth070921-062047.

Fan, L.H., 2016. Study on the Characteristics of Shale Reservoir in Paleogene System in Dongying Sag. China University of Petroleum (East China) in Chinese.

Fang, Z.W., 2016. Characteristics of Mesozoic volcanic reservoirs in Fulin and Qingdong. Special Oil Gas Reservoirs 23 (1), 44–48+153. https://doi.org/10.3969/j.issn.1006-6535.2016.01.010 (in Chinese).

Fisher, R.V., Schmincke, H.U., 1984. Pyroclastic Rocks. Springer-Verlag, Berlin, p. 472.

Gao, P., He, Z.L., Li, S.J., Lash, G.G., Li, B.Y., Huang, B.Y., Yan, D.T., 2018. Volcanic and hydrothermal activities are recorded in phosphate nodules from the lower Cambrian Niutitang formation black shales in South China. Paleogeogr. Paleoclimatol. Paleoecol. 505, 381–397. https://doi.org/10.1016/j.palaeo.2018.06.019.

Guo, X.S., Hu, D.F., Li, Y.P., Duan, J.B., Ji, C.H., Duan, H., 2018. Discovery and theoretical and technical innovations of yuanba gas field in Sichuan Basin, SW China. Petrol. Explor. Dev. 45, 15–28. https://doi.org/10.1016/S1876-3804(18)30002-8.

Guo, X.S., Li, Y.P., Borjigen, T., Wang, Q., Yuan, T., Shen, B.J., Ma, Z.L., Wei, F.B., 2020. Hydrocarbon generation and storage mechanisms of deepwater shelf shales of Ordovician Wufeng formation-Silurian Longmaxi Formation in Sichuan Basin, China. Petrol. Explor. Dev. 47, 204–213. https://doi.org/10.1016/S1876-3804(20)60019-2.

Guo, Y.L., 2011. Basic features of petroleum exploration development in mature exploration area, 2011 Petroleum Geology & Experiment 33 (4), 332–335 (in Chinese).

Hatch, J.R., Leventhal, J.S., 1992. Relationship between inferred redox potential of the depositional environment and geochemistry of the upper Pennsylvanian (Missourian) Stark shale member of the Dennis limestone, Wabaunsee county, Kansas. U.S.A. Chem. Geol. 99, 65–82. https://doi.org/10.1016/0009-2541(92)90031-Y.

Haydon, M., Olivier, J., Thierry, A., Philip, S., Karl, F., Virginie, M., Zsolt, B., Doris, S., 2006. The Cenomanian/Turonian anoxic event at the Bonarelli Level in Italy and Spain: enhanced productivity and/or better preservation? Cretac. Res. 28, 597–612. https://doi.org/10.1016/j.cretres.2006.09.003.

He, Y., Wang, D.Y., Liao, Y.S., 2001. Volcanic rocks, basin evolution and related CO2-Au mineralization in Shengli Oilfield, China. Chin. J. Geol. (Scientia Geologica) 4, 454–464 (in Chinese).

Hong, H.L., Algeo, T.J., Fang, Q., Zhao, L.L., Ji, K.P., Yin, K., Wang, C.W., Cheng, S., 2019a. Facies dependence of the mineralogy and geochemistry of altered volcanic ash beds: an ex-ample from Permian-Triassic transition strata in southwestern China. Earth Sci. Rev. 190, 58–88. https://doi.org/10.1016/j.earscirev.2018.12.007.

Hong, H.L., Zhao, L.L., Fang, Q., Algeo, T.J., Wang, C.W., Yu, J.X., Gong, N.N., Yin, K., Ji, K.P., 2019b. Volcanic sources and diagenetic alteration of Permian-Triassic boundary K-bentonites in Guizhou Province, south China. Paleogeogr. Paleoclimatol. Paleoecol. 519, 141–153. https://doi.org/10.1016/j.palaeo.2018.01.019.

Hou, G.T., Qian, X.L., Song, X.M., 1998. The origin of the Bohai Bay Basin. Acta Sci. Nauralium Univ. Pekin. 34, 503–509. https://doi.org/10.13209/j.0479-8023.1998.033 (in Chinese).

Hou, S.J., 2008. The Research of Deposition System and Evaluation of Beneficial Goal of Shahejie Formation in FuLin Sag. China University of Geosciences, Beijing (in Chinese).

Huff, W.D., 2016. K-bentonites: a review. Am. Mineral. 101, 43–70. https://doi.org/10.2138/am-2016-5339.

Jia, Y.C., Lin, C.S., Eriksson, K.A., Niu, C.M., Li, H.Y., Zhang, P., 2019. Fault control on depositional systems and sequence stratigraphic architecture in a multiphase, rifted, lacustrine basin: a case study from the paleogene of the central Bohai Bay Basin, northeast China. Mar. Petrol. Geol. 101, 459–475. https://doi.org/10.1016/j.marpetgeo.2018.12.019.

Jin, Z.J., Bai, Z.R., Gao, B., Li, M.W., 2019. Has China ushered in the shale oil and gas revolution? Oil Gas Geol. 40 (3), 451–458. https://doi.org/10.11743/ogg20190301 (in Chinese).

Jin, Z.J., Zhu, R.K., Liang, X.P., Shen, Y.Q., 2021. Several issues worthy of attention in current lacustrine shale oil exploration and development. Petrol. Explor. Dev. 48 (6), 1471–1484. https://doi.org/10.11698/PED.2021.06.20 (in Chinese).

Jones, B., Manning, D.A.C., 1994. Comparison of geochemical indices used for the interpretation of paleo-redox conditions in. Chem. Geol. 111, 111–129. https://doi.org/10.1016/0009-2541(94)90085-X.

Kietzmann, D.A., Palma, R.M., 2014. Early Cretaceous crustacean microcoprolites from Sierra de la Cara Cura, Neuquén Basin, Argentina: Taphonomy, environmental distribution, and stratigraphic correlation. Cretaceous Research 49, 214–228. https://doi.org/10.1016/j.cretres.2013.12.008.

Kuypers, M.M.M., Pancost, R.D., Nijenhuis, I.A., Damsté, J.S.S., 2002. Enhanced productivity led to increased organic carbon burial in the euxinic north atlantic basin during the late cenomanian oceanic anoxic event. Paleoceanography 17 (4). https://doi.org/10.1029/2000PA000569, 3-1-3-13.

Li, D.H., Li, J.Z., Huang, J.L., Wang, S.Y., Wang, S.F., 2014. An important role of volcanic ash in the formation of shale plays and its inspiration. Nat. Gas. Ind. 34 (5), 56–65. https://doi.org/10.3787/j.issn.1000-0976.2014.05.006 (in Chinese).

Li, G.F., Li, J.P., Wang, G.Z., Chen, J.C., Gong, H.J., 2009. Control of structure-paleogeomorphology on the deposition of the third member of the paleogene Shahejie Formation in the Qingdong sag of the Bozong depression. Oil Gas Geol. 30, 425–430 (in Chinese).

Little, C.T.S., Herrington, R.J., Maslennikov, V.V., Morris, N.J., Zaykov, V.V., 1997. Silurian hydrothermal-vent community from the southern Urals, Russia. Nature 385, 146–148. https://doi.org/10.1038/385146a0.

Leckie, R.M., Bralower, T.J., Cashman, R., 2002. Oceanic anoxic events and plankton evolution; biotic response to tectonic forcing during the mid-cretaceous. Paleoceanography 17(3),. https://doi.org/10.1029/2001PA000623, 13-1-13-29.

Lee, C.T.A., Jiang, H.H., Ronay, E., Minisini, D., Stiles, J., Neal, M., 2018. Volcanic ash as a driver of enhanced organic carbon burial in the Cretaceous. Sci. Rep. 8 (1), 1-9.10.1038/s41598-018-22576-3.

Liao, Z.W., Hu, W.X., Cao, J., Wang, X.L., Yao, S.P., Wu, H.G., Wan, Y., 2016. Heterogeneous volcanism across the Permian-Triassic boundary in south China and implications for the latest permian mass extinction: new evidence from volcanic ash layers in the lower Yangtze region. J. Asian Earth Sci. 127, 197–210. https://doi.org/10.1016/j.jseaes.2016.06.003.

Liang, C., Wu, J., Jiang, Z.X., Cao, Y.C., Liu, S.J., Pang, S.Y., 2017. Significances of organic matters on shale deposition, diagenesis process, and reservoir formation. J. Chin. Univ. Petrol 41 (6), 1–8. https://doi.org/10.3969/j.issn.1673-5005.2017.06.001 (in Chinese).

Liang, X.P., Jin, Z.J., Liu, Q.Y., Shpilman, A., Li, P., Morozov, V., Uspensky, B., 2021. Impact of volcanic ash on the formation of organic-rich shale: a case study on the Mesozoic Bazhenov formation, West Siberian Basin. Oil Gas Geol. 42 (1), 201–211. https://doi.org/10.11743/ogg20210117 (in Chinese).

Lin, C.S., Zheng, H.R., Ren, J.Y., Liu, J.Y., Qiu, Y.G., 2003. Control of early tertiary synsedimentary faulting on sedimentary filling in Dongying and Zhanhua sag, Bohai Bay Basin. Sci. China Earth Sci. 11 1025-1036.10.1360/03yd0203. (in Chinese).

Liu, D., 2016. Distribution and its main controlling factors of reservoirs of Shahejie formation in Qingdong Sag, Jiyang Depression. In: China University of Petroleum, Beijing (in Chinese).

Liu, J.Y., Liu, Q.Y., Zhu, D.Y., Meng, Q.Q., Liu, W.H., Qiu, R.Y., Huang, Z.K., 2018. The role of deep fluid in the formation of organic-rich source rocks. Nat. Gas Geosci.

29 (2), 168–177. https://doi.org/10.11764/j.jnggs.1672-1926.2017.11.013 (in Chinese).
Liu, H.M., 2022. Exploration practice and prospect of shale oil in Jiyang Depression. China Petrol. Explor. 27, 73–87. https://doi.org/10.3969/j.issn.1672-7703.2022.01.007 (in Chinese).
Liu, H.M., Yang, H.Y., Zhang, P.F., Han, T.X., Liu, X.J., 2022a. Control effect of paleo-lacustrine water conditions on mixed lithofacies assemblages: a case study of the Palaeogene Es3, Dongying Sag, Bohai Bay Basin. Oil Gas Geol. 43, 297–306. https://doi.org/10.11743/ogg20220205 (in Chinese).
Liu, Q.Y., Zhu, D.Y., Jin, Z.J., Meng, Q.Q., Li, S.J., 2019. Influence of volcanic activities on redox chemistry changes linked to the enhancement of the ancient Sinian source rocks in the Yangtze craton. Precambrian Res. 327, 1–13. https://doi.org/10.1016/j.precamres.2019.02.017.
Liu, Q.Y., Zhu, D.Y., Meng, Q.Q., Liu, J.Y., Wu, X.Q., Zhou, B., Fu, Q., Jin, Z.J., 2018. The scientific connotation of oil and gas formations under deep fluids and organic-inorganic interaction. Sci. China Earth Sci. 49 (3), 507–528. https://doi.org/10.1007/s11430-018-9281-2.
Liu, Q.Y., Li, P., Jin, Z.J., Liang, X.P., Zhu, D.Y., Wu, X.Q., Meng, Q.Q., Liu, J.Y., Zhao, J.H., 2021. Preservation of organic matter in shale linked to bacterial sulfate reduction (BSR) and volcanic activity under marine and lacustrine depositional environments. Mar. Petrol. Geol. 127, 104950. https://doi.org/10.1016/j.marpetgeo.2021.104950.
Liu, Q.Y., Li, P., Jin, Z.J., Sun, Y.W., Hu, G., Zhu, D.Y., Huang, Z.K., Liang, X.P., Zhang, R., Liu, J.Y., 2022b. Organic-rich formation and hydrocarbon enrichment of lacustrine shale strata: a case study of Chang 7 Member. Sci. China Earth Sci. 65, 118–138. https://doi.org/10.1007/s11430-021-9819-y.
Liu, X.B., Liu, G.D., Song, Z.Z., Jiang, W.Y., Wang, N., 2022c. The paleo-sedimentary environment and formation mechanism of the source rocks in Shahejie Formation, Qikou sag, Bohai Bay Basin. Nat. Gas Geosci. 33 (12), 2008–2031. https://doi.org/10.11764/j.issn.1672-1926.2022.09.001 (in Chinese).
Ma, L.C., 2014. Characteristics and distribution of reservoirs in Qingdong sag, jiyang depression. Petroleum Geology & Experiment 36, 39–45. https://doi.org/10.11781/sysydz201401039 (in Chinese).
Pan, R.F., Chen, M.L., Zhang, C.M., Shen, L.Y., Yang, B.G., 2016. Characteristics of shale organic matter thermal evolution in Paleogene Shahejie Formation in Jiyang depression. Earth Sci. Front. 23, 277–283. https://doi.org/10.13745/j.esf.2016.04.023 (in Chinese).
Pearson, V.K., Sephton, M.A., Kearsley, A.T., Bland, P.A., Franchi, L.A., Gilmour, L., 2002. Clay mineral-organic matter relationships in the early solar system. Meteorit. Planet. Sci. 37 (12), 1829–1833. https://doi.org/10.1111/j.1945-5100.2002.tb01166.x.
Song, M.S., Li, Y.Q., 2020. Evaluation and practice of fine petroleum exploration in the Jiyang Depression. China Petroleum Exploration 25 (1), 93–101. https://doi.org/10.3969/j.issn.1672-7703.2020.01.009 (in Chinese).
Shi, J.Y., Jin, Z.J., Liu, Q.Y., Huang, Z.K., 2020. Depositional process and astronomical forcing model of lacustrine fine-grained sedimentary rocks; a case study of the early Paleogene in the Dongying Sag, Bohai Bay Basin. Mar. Petrol. Geol. 113, 103995. https://doi.org/10.1016/j.marpetgeo.2019.08.023.
Su, B., Cao, Z.C., Shi, Z.J., 2015. Exploration of earth-abundant transition metals (Fe, Co, and Ni) as catalysts in unreactive chemical bond activations. Accounts Chem. Res. 48, 886–896. https://doi.org/10.1021/ar500345f.
Taylor, S.R., Mclennan, S.M., 1985. The Continental Crust: Lts Composition and Evolution. Blackwell Scientific Publications, Oxford.
Tian, L.X., Wang, Q.B., Liu, X.J., Hao, Y.W., 2020. Geological features and their participation in the formation of silicified clastic reservoirs in the Shahejie Formation of Laizhouwan Sag, Bohai Sea. Oil Gas Geol. 41, 1073–1082. https://doi.org/10.11743/ogg20200517 (in Chinese).
Trowbridge, A., Walton, S.M., Gaunt, M.J., 2020. New strategies for the transition-metal catalyzed synthesis of aliphatic amines. Chem. Rev. 120, 2613–2692. https://doi.org/10.1021/acs.chemrev.9b00462.
Verati, C., De, D.P., Prieur, D., Lancelot, J., 1999. Evidence of bacterial activity from micrometer-scale layer analyses of black-smoker sulfide structures (pito seamount site, easter microplate). Chem. Geol. 158 (3–4), 257–269. https://doi.org/10.1016/S0009-2541(99)00054-6.
Wang, J.F., Han, W.G., Yu, J.G., Zhen, J.B., 2003. Turbidity system in the third section of Shahejie Formation of Dongying Sag and its implications on petroleum prospecting. Acta Pet. Sin. 6, 24–29 (in Chinese).
Wang, S.H., Xia, B., Chen, G.W., Jiang, Z.X., Xiao, S.B., Yu, J.F., 2004. Characteristics of jiyang depression and mechanism of basin formation. Geotect. Metallogenia 4, 428–434. https://doi.org/10.16539/j.ddgzyckx.2004.04.009 (in Chinese).
Wang, M., Wilkins, R.W.T., Song, G.Q., Zhang, L.Y., Xu, X.Y., Li, Z., Chen, G.H., 2015. Geochemical and geological characteristics of the Es3L lacustrine shale in the bonan sag, Bohai Bay Basin, China. Int. J. Coal Geol. 138 (15), 16–29. https://doi.org/10.1016/j.coal.2014.12.007.
Wang, M., Li, X.P., Dai, X.G., 2016. Thermal evolution characteristics of Triassic coal in Chuxiong Basin and its geological significance. Int. J. Min. Sci. Technol. 26 (5), 937–945. https://doi.org/10.1016/j.ijmst.2016.05.035.
Wang, M., Ma, R., Li, J.B., Lu, S.F., Li, C.M., Guo, Z.Q., Li, Z., 2019. Occurrence mechanism of lacustrine shale oil in the paleogene Shahejie Formation of jiyang depression, Bohai Bay Basin, China. Petrol. Explor. Dev. 46, 789–802. https://doi.org/10.11698/PED.2019.04.19 (in Chinese).
Wang, Y., Lu, K.Z., Ren, A.S., 1994. Mesozoic tectonism and volcanism in the northeastern Jiyang Depression and basin evolution. J. Chin. Univ. Petrol 2, 1–8 (in Chinese).
Wu, L.Y., Lu, Y.C., Jiang, S., Liu, X.F., He, G.S., 2018. Effects of volcanic activities in ordovician Wufeng-Silurian longmaxi period on organic-rich shale in the upper Yangtze area, south China. Petrol. Explor. Dev. 45, 806–816. https://doi.org/10.11698/PED.2018.05.06 (in Chinese).
Wu, L.G., Li, X.S., Guo, X.B., Luo, Q.S., Liu, X.J., Chen, X., Jiang, Z.X., 2012. Diagenetic evolution and formation mechanism of dissolved pore of shale oil reservoirs of Lucaogou formation in Malang sag. J. Chin. Univ. Petrol 36, 38–43. https://doi.org/10.3969/j.issn.1673-5005.2012.03.007 (in Chinese).
Xie, H.R., Liang, C., Wu, J., Ji, S.C., 2023. Impact of volcanica activity on editorial paleo environmental and organic matter enrich. J. Palaegeogr. (Chinese Edition) 4, 1–20. https://doi.org/10.7605/gdlxb.2023.04.066 (in Chinese).
Xu, H.Y., George, S.C., Hou, D.J., 2019. Algal-derived polycyclic aromatic hydrocarbons in paleogene lacustrine sediments from the dongying depression, Bohai Bay Basin, China. Mar. Petrol. Geol. 102, 402–425. https://doi.org/10.1016/j.marpetgeo.2019.01.004.
Yang, G., 2011. Structural framework and evolution of Qingdong sag, Bohai Bay Basin. Petrol. Geol. and Recovery 18 (1), 7–10. https://doi.org/10.13673/j.cnki.cn37-1359/te.2011.01.012 (in Chinese).
Yu, T., Wang, D., Dong, H.L., Zeng, Q., 2014. Effects of microbial iron reduction by A sulfate-reducing bacterium on the preservation of organic matter in nontronite. Bull. China Soc. Mineral Petrol. Geochem. 33 (6), 790–796. https://doi.org/10.3969/j.issn.1007-2802.2014.06.006 (in Chinese).
Zhao, J.H., Jin, Z.J., Jin, Z.K., Xin, W., Geng, Y.K., Yan, C.N., 2015. Characteristics of biogenic silica and its effect on reservoir in Wufeng-Longmaxi shales, Sichuan basi. Acta Geol. Sin. 89 (S1), 139. https://doi.org/10.1111/1755-6724.12302-58.
Zhang, L.M., Wang, C.S., Wignall, P.B., Kluge, T., Wan, X.Q., Wang, Q., Gao, Y., 2018. Deccan volcanism caused coupled pCO_2 and terrestrial temperature rises, and pre-impact extinctions in northern China. Geology 46 (3), 271–274. https://doi.org/10.1130/G39992.1.
Zhou, L.H., Han, G.M., Ma, J.Y., Chen, C.W., Yang, F., Zhang, L.H., Zhou, K.J., Chen, S.Q., Yang, F., Dong, Y.Q., Zhou, J., 2020. Palaeoenvironment characteristics and sedimentary model of the lower submember of Member 1 of Shahejie Formation in the southwestern margin of Qikou sag. Acta Pet. Sin. 41 (8), 903–917. https://doi.org/10.7623/syxb202008001 (in Chinese).
Zeng, Q., Dong, H.L., Zhao, L.D., Huang, Q.Y., 2016. Preservation of organic matter in nontronite against iron redox cycling. Am. Mineral. 101, 120–133. https://doi.org/10.2138/am-2016-5410.
Zou, C.N., Zhu, R.K., Chen, Z.Q., Ogg, J.G., Wu, S.T., Dong, D.Z., Qiu, Z., Wang, Y.M., Lan, W., Lin, S.H., Cui, J.W., Su, L., Yang, Z., 2019. Organic-matter-rich shales of China. Earth Sci. Rev. 189, 51–78. https://doi.org/10.1016/j.earscirev.2018.12.002.